

Is $N = 2$ Large?

Ryuichiro Kitano^{1,2,*}, Norikazu Yamada^{1,2,†} and Masahito Yamazaki^{3‡}

¹ *High Energy Accelerator Research Organization (KEK), Tsukuba 305-0801, Japan*

² *Graduate University for Advanced Studies (SOKENDAI), Tsukuba 305-0801, Japan*

³ *Kavli Institute for the Physics and Mathematics of the Universe (WPI),*

University of Tokyo, Kashiwa, Chiba 277-8583, Japan

(Dated: February 10, 2021)

Abstract

We study θ dependence of the vacuum energy for the 4d SU(2) pure Yang-Mills theory by lattice numerical simulations. The response of topological excitations to the smearing procedure is investigated in detail, in order to extract topological information from smeared gauge configurations. We determine the first two coefficients in the θ expansion of the vacuum energy, the topological susceptibility χ and the first dimensionless coefficient b_2 , in the continuum limit. We find consistency of the SU(2) results with the large N scaling. By analytic continuing the number of colors, N , to non-integer values, we infer the phase diagram of the vacuum structure of SU(N) gauge theory as a function of N and θ . Based on the numerical results, we provide quantitative evidence that 4d SU(2) Yang-Mills theory at $\theta = \pi$ is gapped with spontaneous breaking of the CP symmetry.

*Electronic address: ryuichiro.kitano@kek.jp

†Electronic address: norikazu.yamada@kek.jp

‡Electronic address: masahito.yamazaki@ipmu.jp

Contents

I. Introduction	2
II. Lattice Simulations	4
A. Lattice Setup	5
B. Smearing and Definition of Topological Charges on the Lattice	6
C. Response to Smearing	7
D. Results	13
III. Discussion	18
A. Large N versus Small N	18
1. Large N	18
2. Small N	20
3. Intermediate N	22
4. Comparison with the CP^{N-1} Model	24
B. Quantitative Analysis of Lattice Results	25
1. $N = 2$	25
2. N_{inst}	26
IV. Summary and Discussion	28
Acknowledgments	29
References	29

I. INTRODUCTION

The θ term of the Yang-Mills theory determines how to weight different topological sectors in the path integral. Since the θ parameter is the coefficient of a total derivative term in the Lagrangian, the θ -dependences of observables can be explored only through non-perturbative methods.

The special value $\theta = \pi$ has been of particular interest. In the classic literature [1–3], spontaneous CP violation of the 4d $SU(N)$ Yang-Mills theory at $\theta = \pi$ was demonstrated

in the large N limit [4]. More recently, an anomaly matching argument involving generalized global symmetries [5] showed that the CP symmetry in the confining phase has to be broken even at finite N [6]. A similar conclusion was derived by studying restoration of the equivalence of local observables between $SU(N)$ and $SU(N)/Z_N$ gauge theories in the infinite volume limit [7]. See, for example, Refs. [8–10] for other approaches.

While lattice numerical simulations are ideal tools to explore non-perturbative dynamics of gauge theories, direct simulations at $\theta = \pi$ has been challenging due to the notorious sign problem.¹ Nevertheless, lattice simulations have been successfully used to determine the first few coefficients in the θ expansion of the vacuum energy for finite N . On the one hand, below the critical temperature T_c these coefficients turn out to be consistent with the large N scaling down to $N = 3$ [14–16], which indicates spontaneous CP violation and the discontinuity of the vacuum energy across $\theta = \pi$. On the other hand, above T_c the coefficients determined at $N = 3$ and 6 are found to be consistent with the dilute instanton gas approximation (DIGA) [17], which predicts continuous behavior for the vacuum energy across $\theta = \pi$.

The CP^{N-1} model in two dimensions shares many non-perturbative properties with the four-dimensional $SU(N)$ Yang-Mills theory [18, 19], and hence provides useful insights into the latter. For $N \geq 3$, the model is believed to show spontaneous CP violation at $\theta = \pi$ [20]. By contrast the case with $N = 2$ is believed to be special and argued to become gapless at $\theta = \pi$ with unbroken CP symmetry [21–29]. Motivated by similarities between the 4d Yang-Mills theory and the 2d CP^{N-1} model, it is natural to ask if the 4d $SU(N)$ Yang-Mills theory at $\theta = \pi$ shows distinctive behavior for small values of N , such as $N = 2$.²

In this work we explore the θ dependence of the vacuum energy of the 4d $SU(2)$ pure Yang-Mills gauge theory. In sec. II, we perform lattice numerical calculations to determine the first two coefficients in the θ expansion of the vacuum energy. The response of topological excitations to the smearing procedure is investigated in detail, in order to efficiently extract physical information from lattice configurations. The coefficients determined for $N = 2$ are compared to those previously obtained for $N \geq 3$, to see whether the result at $N = 2$ can be seen as a natural extrapolation of those for $N \geq 3$. In sec. III, we begin with theoretical

¹ Recent and related developments towards direct simulations are found, for example, in Refs. [11–13].

² The \mathbb{Z}_N subgroup of the flavor symmetry of the 2d CP^{N-1} model can be regarded as a counterpart of the 1-form \mathbb{Z}_N center symmetry of the 4d $SU(N)$ pure Yang-Mills theory.

arguments for different behaviors of 4d $SU(N)$ theory, for large N and for small N as we analytically continue the values of N . We then interpret the numerical results of sec. II and provide quantitative evidence that the 4d $SU(2)$ theory belongs to the “large N ” class, and is gapped and has spontaneous breaking of CP symmetry at $\theta = \pi$.

II. LATTICE SIMULATIONS

The vacuum energy can be expanded around $\theta = 0$ as

$$E(\theta) - E(0) = \frac{\chi}{2} \theta^2 (1 + b_2 \theta^2 + b_4 \theta^4 + \dots) , \quad (1)$$

where χ is the topological susceptibility, and b_{2i} ($i = 1, 2, 3, \dots$) are dimensionless coefficients describing the deviation of the topological charge distribution from the Gaussian. These quantities can be determined from the lattice configurations generated at $\theta = 0$ as

$$\chi = \frac{\langle Q^2 \rangle_{\theta=0}}{V} , \quad (2)$$

$$b_2 = -\frac{\langle Q^4 \rangle_{\theta=0} - 3 \langle Q^2 \rangle_{\theta=0}^2}{12 \langle Q^2 \rangle_{\theta=0}} , \quad (3)$$

$$b_4 = \frac{\langle Q^6 \rangle_{\theta=0} - 15 \langle Q^2 \rangle_{\theta=0} \langle Q^4 \rangle_{\theta=0} + 30 \langle Q^2 \rangle_{\theta=0}^3}{360 \langle Q^2 \rangle_{\theta=0}} , \quad (4)$$

where Q is the topological charge, whose precise definition is given in eqs. (10)-(14), and $\langle \dots \rangle_{\theta=0}$ denotes an ensemble average over configurations generated at $\theta = 0$. According to the large N analysis [1, 3], these quantities can be expressed, as a function of N , as

$$\chi(N) = \chi(\infty) + O(N^{-2}) , \quad (5)$$

$$b_{2i}(N) = \frac{b_{2i}^{(1)}}{N^{2i}} + O\left(\frac{1}{N^{2i+2}}\right) . \quad (6)$$

By contrast the dilute instanton gas approximation leads to $E(\theta) - E(0) = \chi(1 - \cos \theta)$, and hence the coefficients, $b_2^{\text{DIGA}} = -1/12$, $b_4^{\text{DIGA}} = 1/360$, \dots , are completely determined. We attempted calculating b_4 as well as χ and b_2 . We could obtain only a loose bound $-0.1 < b_4 < 0.1$ due to a large statistical uncertainty. In the following, we focus on the determinations of χ and b_2 .

β	N_S	N_{T_c}	$(aT_c)^2$	$L\sigma_{\text{str}}^{1/2}$	statistics
1.750	16	4.65	0.0462	4.9	80,100
1.850	16	6.50	0.0237	3.5	71,040
1.975	16	9.50	0.0111	2.4	30,490
1.975	24	9.50	0.0111	3.6	131,830

TABLE I: The simulation parameters. T_c denotes the critical temperature. N_{T_c} is determined from Ref. [31]. The uncertainties of N_{T_c} are below 1% and hence neglected in the following.

A. Lattice Setup

The SU(2) gauge action on the lattice is described as

$$S_g = 6\beta N_{\text{site}} \{c_0(1 - W_P) + 2c_1(1 - W_R)\} , \quad (7)$$

where $\beta = 4/g^2$ is the lattice gauge coupling, W_P and W_R are the 1×1 plaquette and the 1×2 rectangle averaged over four dimensional lattice sites, respectively, and c_0 and c_1 satisfying $c_0 = 1 - 8c_1$ are the improvement coefficients. We take the tree-level Symanzik improved action [30], which is realized by $c_1 = -1/12$. To investigate the continuum limit, three values of the lattice coupling ($\beta=1.750, 1.850$ and 1.975) are taken. The lattice size is $N_{\text{site}} = N_S^3 \times N_T$ with $N_S = 16$ and $N_T = 2 \times N_S$. We also perform simulations with $N_S = 24$ on our finest lattice to check finite volume effects. The lattice spacing at each β is taken from $N_{T_c} = 1/(a(\beta)T_c)$ obtained in Ref. [31], where T_c is the critical temperature for the SU(2) pure Yang-Mills theory. The value N_{T_c} is then transformed to $(aT_c)^2$ for later use. To have an intuition about how large our lattice is, we estimated $L\sigma_{\text{str}}^{1/2}$ at each lattice, using $T_c/\sqrt{\sigma_{\text{str}}} = 0.7091(36)$ [32], where L denotes the physical length of the spatial direction, *i.e.* $L = aN_S$, and σ_{str} is the representative dynamical scale (the string tension). Gauge configurations are generated by hybrid Monte Carlo method and are stored every 10 trajectories. Simulation parameters including the lattice spacings, the lattice size and the number of configurations (denoted as statistics in the table) are summarized in Tab. I.

B. Smearing and Definition of Topological Charges on the Lattice

Among several equivalent methods often used in the literature [33–35], we choose the combination of the APE smearing [36] and the 5-loop improved operator [37] to calculate topological charge on each configuration. Topological charges on the lattice are obscured by short distance fluctuations, which we remove by introducing a smoothing technique. In the APE smearing, new link variables $U_\mu^{(\text{new})}$ are constructed from old ones $U_\mu^{(\text{old})}$ as

$$U_\mu^{(\text{new})} = \text{Proj} \left[(1 - \rho) U_\mu^{(\text{old})}(x) + \rho X_\mu(x) \right] , \quad (8)$$

$$X_\mu(x) = \sum_{\nu \neq \mu} \left[U_\nu^{(\text{old})}(x) U_\mu^{(\text{old})}(x + \hat{\nu}) U_\nu^{(\text{old})\dagger}(x + \hat{\mu}) \right. \\ \left. + U_\nu^{(\text{old})\dagger}(x - \hat{\nu}) U_\mu^{(\text{old})}(x - \hat{\nu}) U_\nu^{(\text{old})}(x - \hat{\nu} + \hat{\mu}) \right] , \quad (9)$$

where Proj acts as the projection back to an SU(2) element. This procedure minimizes the action density. The parameter ρ is taken to be 0.2, which corresponds to $\alpha_{\text{APE}} = 6\rho/(1 + 5\rho) = 0.6$ in Ref. [35].

The 5-loop improved topological charge operator is given by

$$Q = \sum_x q(x) , \quad (10)$$

$$q(x) = \sum_i c_i q_{m_i, n_i}(x) , \quad (11)$$

$$q_{m, n}(x) = \frac{1}{32\pi^2} \frac{1}{m^2 n^2} \sum_{\mu, \nu, \rho, \sigma} \epsilon_{\mu, \nu, \rho, \sigma} \text{Tr} \left[\hat{F}_{\mu, \nu}(x; m, n) \hat{F}_{\rho, \sigma}(x; m, n) \right] , \quad (12)$$

$$\hat{F}_{\mu, \nu}(x; m, n) = \frac{1}{8} \text{Im} \left[\{ \text{oriented clover average of } (m \times n) \text{ plaquette} \} + \{ (m \leftrightarrow n) \} \right] , \quad (13)$$

where $(m_i, n_i) = (1, 1), (2, 2), (1, 2), (1, 3), (3, 3)$ for $i = 1, \dots, 5$ and the coefficients are given by

$$c_1 = (19 - 55c_5)/9, \quad c_2 = (1 - 64c_5)/9, \quad c_3 = (-64 + 640c_5)/45, \\ c_4 = 1/5 - 2c_5, \quad c_5 = 1/20 . \quad (14)$$

This operator is free of $O(a^2)$ and $O(a^4)$ terms. The replacement above is done once for all link variables, for each step of the smearing. The smearing is carried out every 10 trajectories, and the topological charge is measured after every smearing step.

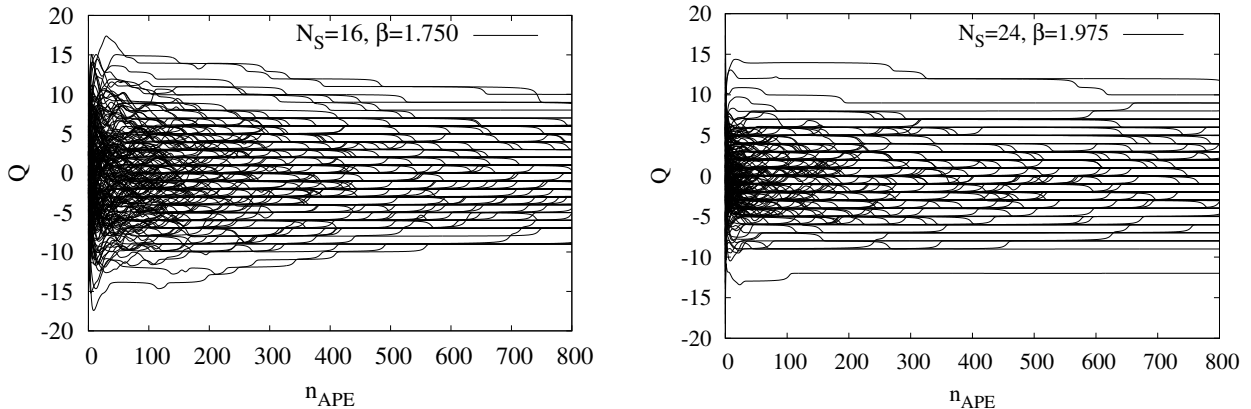


FIG. 1: Smearing history of topological charge Q as a function of the number of smearing steps n_{APE} for randomly chosen 200 configurations at $\beta = 1.750$ and 1.975 .

C. Response to Smearing

As mentioned above, the smearing is introduced to remove short distance fluctuations, which distort physical topological excitations through local lumps with the size of the lattice spacing. The measurement of the topological charge is therefore reliable only after a suitable number of smearing steps. However, the smearing may also affect physical topological excitations. The previous dedicated studies revealed that the smearing induces pair-annihilation, “melting away” or “falling through the lattice” [37–39]. In Ref. [39], it was found that topological objects go through several characteristic phases during the cooling procedure. In the first phase, the size of topological objects grows with the cooling, and some of them eventually melt away and some pair-annihilate. Then, the second phase comes where only relatively slow shrinkage of the objects takes place and eventually they disappear after long enough cooling. Assuming that the similar phases show up in the procedure of APE smearing, we will in the following determine the boundary between the two phases.

In order to explore how the smearing changes topological properties, we first look at the smearing history of the topological charge Q as a function of the smearing steps n_{APE} . Fig. 1 shows the history obtained at $\beta = 1.750$ and 1.975 . At relatively small n_{APE} , Q changes frequently, and most of the changes here are expected to be associated with the removal of short distance fluctuations. We deduce that this range of n_{APE} corresponds to the first phase. The frequency of change in Q is somewhat reduced as n_{APE} and β increase, but the

change steadily continues. In this region, both the increase and the decrease of Q happen mostly by one unit, and a change takes $O(10)$ steps to be completed. This range of n_{APE} is identified with the second phase. In the following, we discuss quantitative differences between the two phases.

We studied the correlation between the topological charge Q and the value of the action S_g . At the same time, we also investigated the direction of change of Q per one step of the smearing, by classifying each configuration at a given n_{APE} into three classes:

- “*stable*” if the change is small, *i.e.* $|Q(n_{\text{APE}}) - Q(n_{\text{APE}} - 1)| \leq 0.05$.

If not stable,

- “*decreasing*” if $Q(n_{\text{APE}})$ is approaching zero,
- “*increasing*” if $Q(n_{\text{APE}})$ is moving away from zero.

Fig. 2 shows the scatter plot for Q and S_g at several values of n_{APE} , obtained at $\beta = 1.750$, where the Bogomolnyi bound, $S_g = 8\pi^2|Q|/g^2$ is shown by dotted lines. The “*stable*”, “*decreasing*” and “*increasing*” data points are shown in blue, red and green, respectively. There is no qualitative difference in the same plot for other values of β . It is seen that points gradually accumulate on integer values of Q by “*increasing*” or “*decreasing*”. The value of the action is never below the Bogomolnyi bound in each topological sector, as expected. This indicates that “*increasing*” data can not exist around the boundary because the smearing lowers the action value and only either instantons(s) or anti-instanton(s) can exist on the bound. It is also seen that the larger the value of $|Q|$ is, faster the minimum of the action in the topological sector reaches the Bogomolnyi bound. Thus, the minimum value of S_g in the $Q = 0$ sector arrives at the bound, *i.e.* $S_g = 0$, last.

Instantons are known to saturate the Bogomolnyi bound. Therefore, the data points with nonzero Q around the bound are attributed to approximate instantons or anti-instantons, and the “*decreasing*” occurring around there are interpreted as (anti-) instantons “falling through the lattice”. We expect that all the “*increasing*” and “*decreasing*” in the second phase are caused by “falling”. In order to examine this expectation, we introduce the

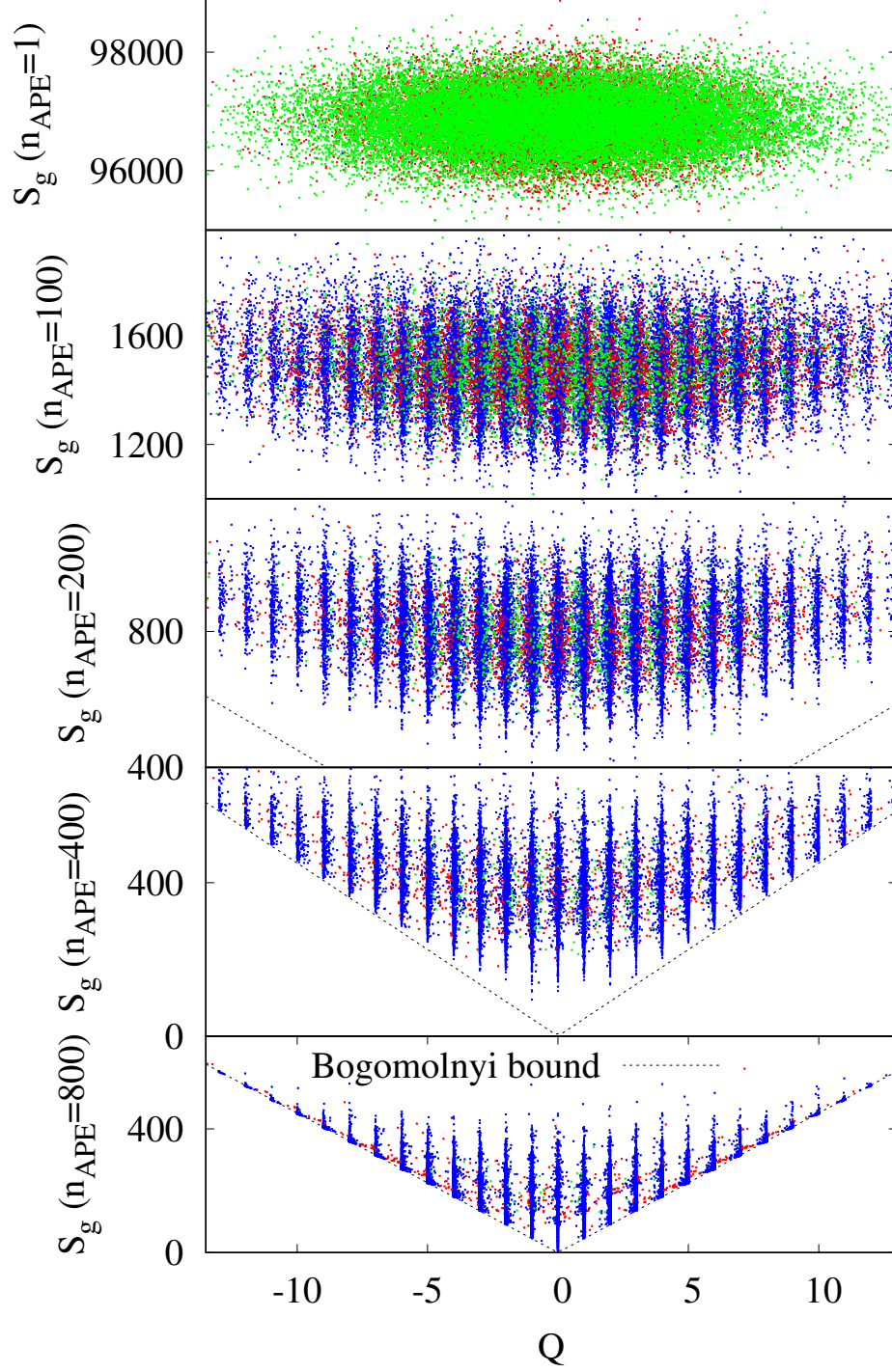


FIG. 2: Correlation between the topological charge Q and the action S_g at smearing steps $n_{\text{APE}} = 1, 100, 200, 400, 800$ (from top to bottom) at $\beta = 1.750$. Blue, red, and green dots represent the configurations in which $|Q|$ are “stable”, “decreasing”, and “increasing”. The dotted lines represent the Bogomolnyi bound.

participation ratio defined by

$$P(n_{\text{APE}}) := \frac{1}{N_{\text{site}}} \frac{\left(\sum_x q(x, n_{\text{APE}})^2 \right)^2}{\sum_x q(x, n_{\text{APE}})^4}, \quad (15)$$

where $q(x, n_{\text{APE}})$ denotes the topological charge density $q(x)$ in eq. (11) after n_{APE} steps of smearing. The participation ratio takes a value between $1/N_{\text{site}}$ and 1. The maximal value $P(n_{\text{APE}}) = 1$ is realized when $q(x, n_{\text{APE}})$ takes a flat distribution over the whole space-time. On the other hand, the possible minimum value, $1/N_{\text{site}}$, is attained when the density forms a local peak, $q(x, n_{\text{APE}}) = \delta(x)$. Fig. 3 shows the smearing history of Q and $\ln P$ as a function of n_{APE} for one particular configuration at $\beta = 1.850$. For $n_{\text{APE}} \gtrsim 30$, whenever Q changes, $\ln P$ shows a rapid increase after slow decrease over many smearing steps. This can be interpreted as that a local object in topological charge density gradually shrinks and suddenly disappears at some point with a change of Q . This is precisely what happens when the “falling through the lattice” occurs [39].

We can directly check this interpretation by studying the distribution of the topological charges. Fig. 4 shows the topological charge density, projected onto the z - t plane, of the

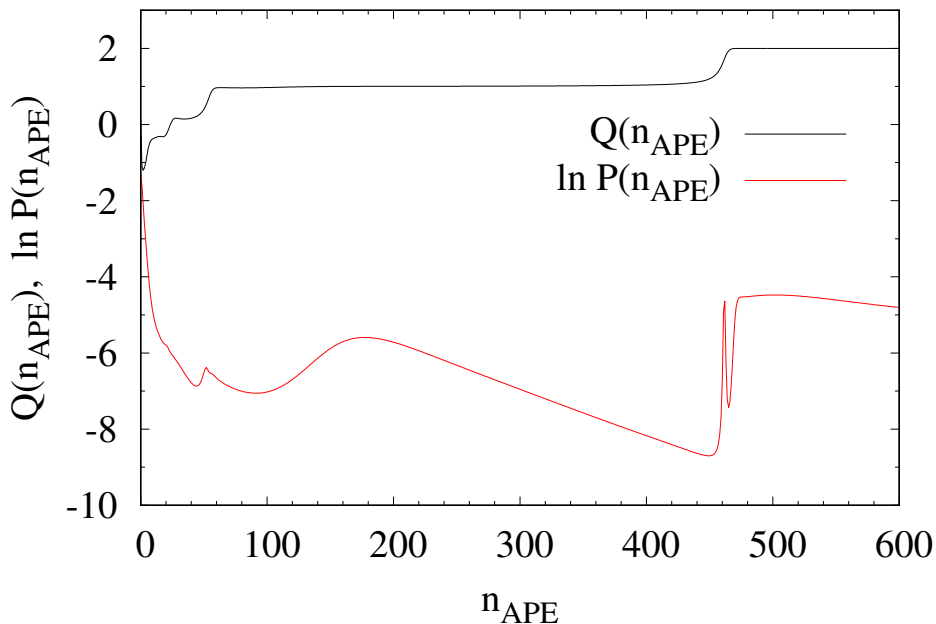


FIG. 3: An example of $Q(n_{\text{APE}})$ and $\ln P(n_{\text{APE}})$ as a function of n_{APE} at $\beta = 1.850$.

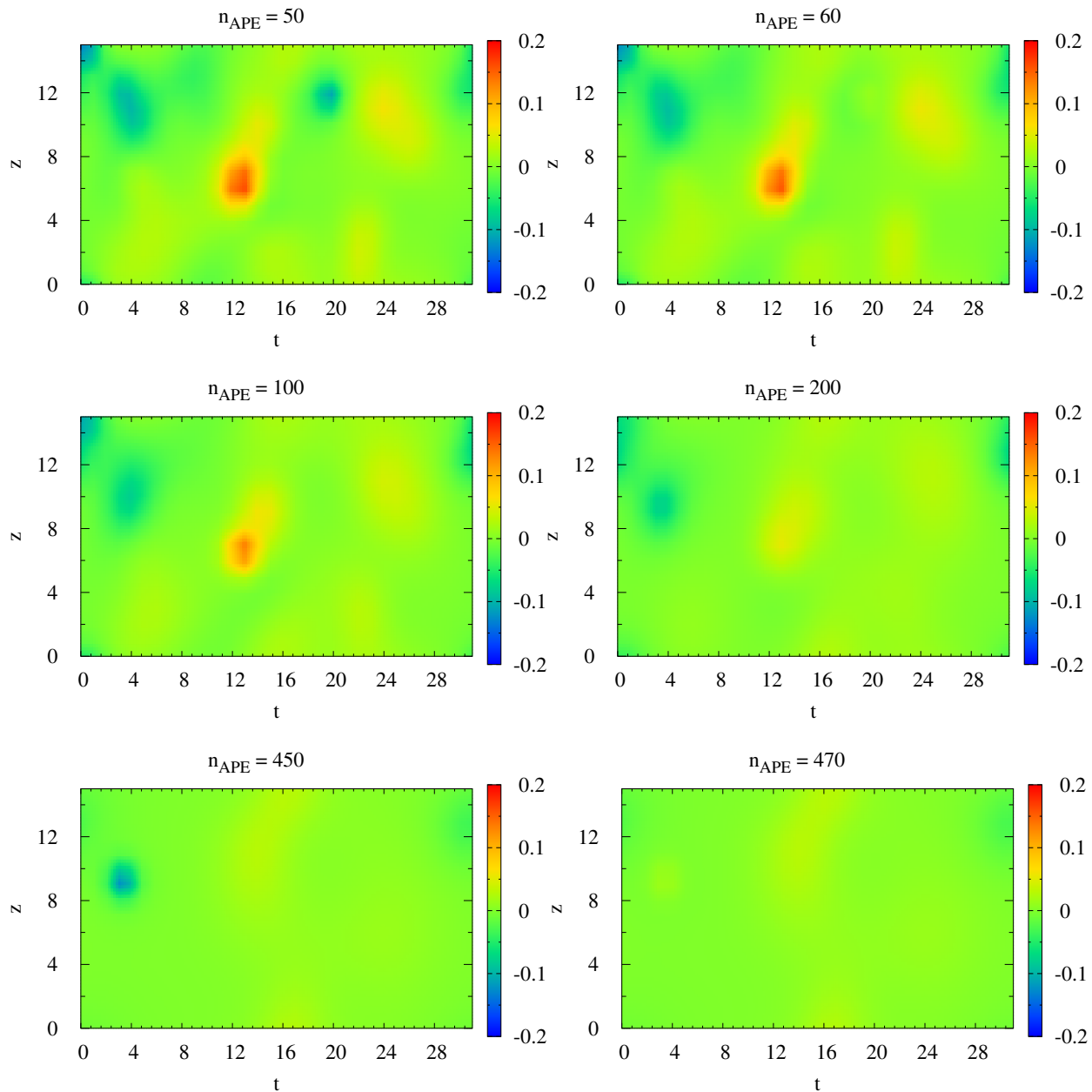


FIG. 4: Distribution of topological charge projected onto $z-t$ plane at $n_{\text{APE}} = 50, 60, 100, 200, 450,$ and 470 .

same configuration as in Fig. 3. Between $n_{\text{APE}} = 50$ and 60 and $n_{\text{APE}} = 450$ and 470 , Q increases by unity, at the same time a negative peak disappears. Between $n_{\text{APE}} = 100$ and 200 , a positive peak seems to be smeared but does not suddenly disappear. It seems that a

complicated process such as a pair annihilation happens in the latter case.

From these observations, we conclude that the changes of Q occurring in the second phase are dominated by the “falling” of instantons or anti-instantons. We expect that the “falling” occurs also in the first phase, but it is overshadowed by changes originating from other reasons.

Instanton and anti-instantons will “fall” at an equal rate. In configurations with $Q > 0$, more instantons exist than anti-instantons and vice versa. Then, it is expected that the “decreasing” would happen more frequently than the “increasing” in the second phase. To see if this is the case, we calculate the ensemble average of

$$\Delta Q(n_{\text{APE}}) = \begin{cases} Q(n_{\text{APE}} + 1) - Q(n_{\text{APE}}) & \text{for } Q(n_{\text{APE}}) > 0 \\ Q(n_{\text{APE}}) - Q(n_{\text{APE}} + 1) & \text{for } Q(n_{\text{APE}}) < 0 \end{cases}. \quad (16)$$

The sign of $\Delta Q(n_{\text{APE}})$ tells us which of “increasing” or “decreasing” happens when going from n_{APE} to $n_{\text{APE}} + 1$. Fig. 5 shows the n_{APE} dependence of $|\langle \Delta Q(n_{\text{APE}}) \rangle|$, where the symbols are filled when its original value is negative. The results from four ensembles

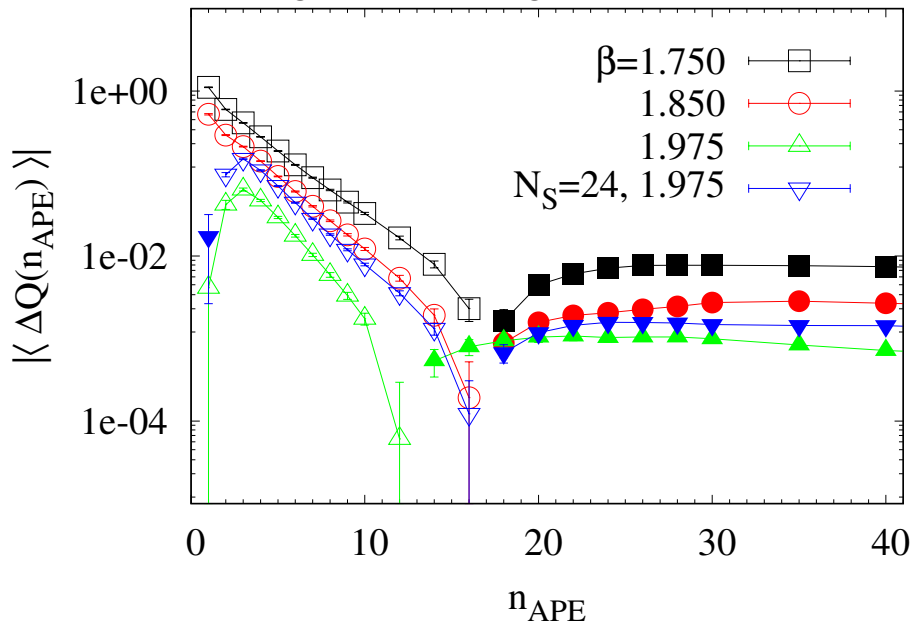


FIG. 5: The *decay rate* of the topological charge.

show exponential fall with approximately a common exponent for $n_{\text{APE}} \lesssim 10$, while they take almost constant negative values for $n_{\text{APE}} \gtrsim 20$. The result for $\beta = 1.975$ and $N_S =$

16 (triangle-up) shows slightly different behaviors probably because of the small physical volume. At any rate, this plot clearly shows that the boundary separating the two phases is located $n_{\text{APE}} \sim 20$. In the following analysis, we only deal with the data for $n_{\text{APE}} \geq 20$, where the short distance fluctuations are gone.

Before closing this subsection, let us add one comment. In Ref. [40], the shape of topological objects in SU(3) gauge theory is examined, and low dimensional long range structures rather than local lumps are discovered. Note that the analysis presented above does not indicate anything about the shape because the smearing changes it. Clearly, it is interesting to perform a similar study in the SU(2) case because the analysis performed in Refs. [41, 42] suggests that the structure could be more localized for SU(2) than for SU(3).

D. Results

Fig. 6 shows the Monte Carlo history of Q over a thousand configurations in four ensembles obtained at $n_{\text{APE}} = 800$. It is seen that the fluctuation of Q is frequent enough, and that the amplitude depends on β and N_{site} . In the following analysis, all the measurements are binned with the bin size of 100 configurations, and a single elimination jackknife method is used to estimate statistical uncertainties.

Fig. 7 shows the histogram of Q for four ensembles at $n_{\text{APE}} = 0, 20, 100$. Approximate Gaussian shape is seen in all ensembles.

Fig. 8 shows the topological susceptibility in lattice unit, $a^4\chi(n_{\text{APE}}) = \langle Q^2 \rangle / N_{\text{site}}$, as a function of n_{APE} . A mild decrease is seen for $n_{\text{APE}} \geq 20$ as expected from a negative constant observed in Fig. 5. We determine topological susceptibility at each lattice by extrapolating the smeared data in the second phase to $n_{\text{APE}} \rightarrow 0$ because the “falling” is supposed to take place even in the first phase. The data points in $n_{\text{APE}} \in [20, 40]$ are well described by a linear function,

$$a^4\chi(n_{\text{APE}}) = a^4\chi(0) + c_1 n_{\text{APE}} . \quad (17)$$

The fit results are tabulated in Tab. II.

Fig. 9 shows n_{APE} dependence of b_2 . Since b_2 is found to be constant for $n_{\text{APE}} \geq 20$, we perform the constant fit to extract b_2 at $n_{\text{APE}} = 0$. The fit results are shown in Tab. II.

The values of b_2 obtained at $\beta = 1.975$ with two lattice volumes turns out to be consistent

with each other due to the large statistical uncertainty, while 1.8σ difference is observed for χ . In Ref. [15, 16], these quantities are calculated with several different volumes for $SU(N)$ with $N = 3, 4, 6$ down to $L \sigma_{\text{str}} \sim 2.5$, and no finite volume effect is observed. Our lattice with $\beta = 1.975$ and $N_S = 16$ corresponds to $L \sigma_{\text{str}} = 2.4$ (see Tab. I), which is smaller than but close to 2.5 and hence finite volume effects, if any, should not be significant. Thus, 1.8σ difference observed at $\beta = 1.975$ is considered as a statistical fluctuation, and we include both results in the following analysis.

Next we discuss the continuum limit. Fig. 10 shows the extrapolation of χ/T_c^4 and b_2 to the continuum. The limit for both quantities is examined by applying two functional forms:

1. constant excluding the coarsest lattice
2. linear in a^2 using all lattices .

The constant fit is used to estimate the continuum limit assuming no scaling violation for the finer lattices, whereas the linear fit including the coarsest lattice serves to probe the

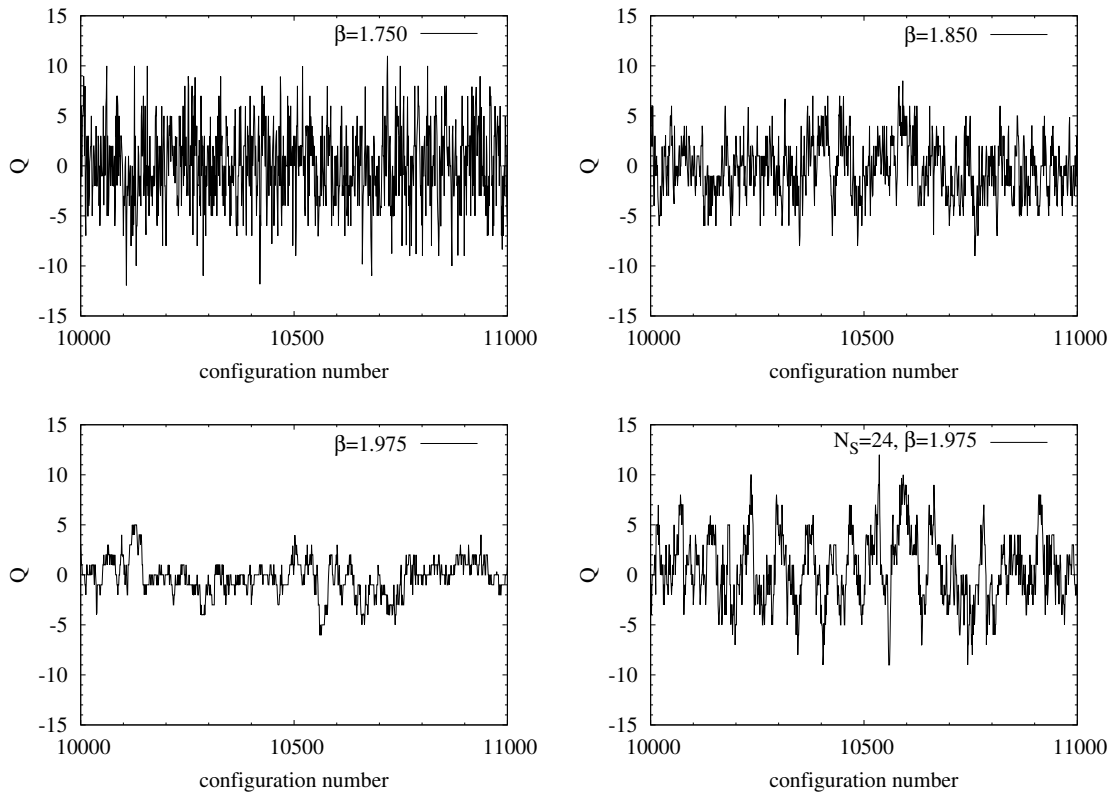


FIG. 6: Monte Carlo history of Q at four ensembles.

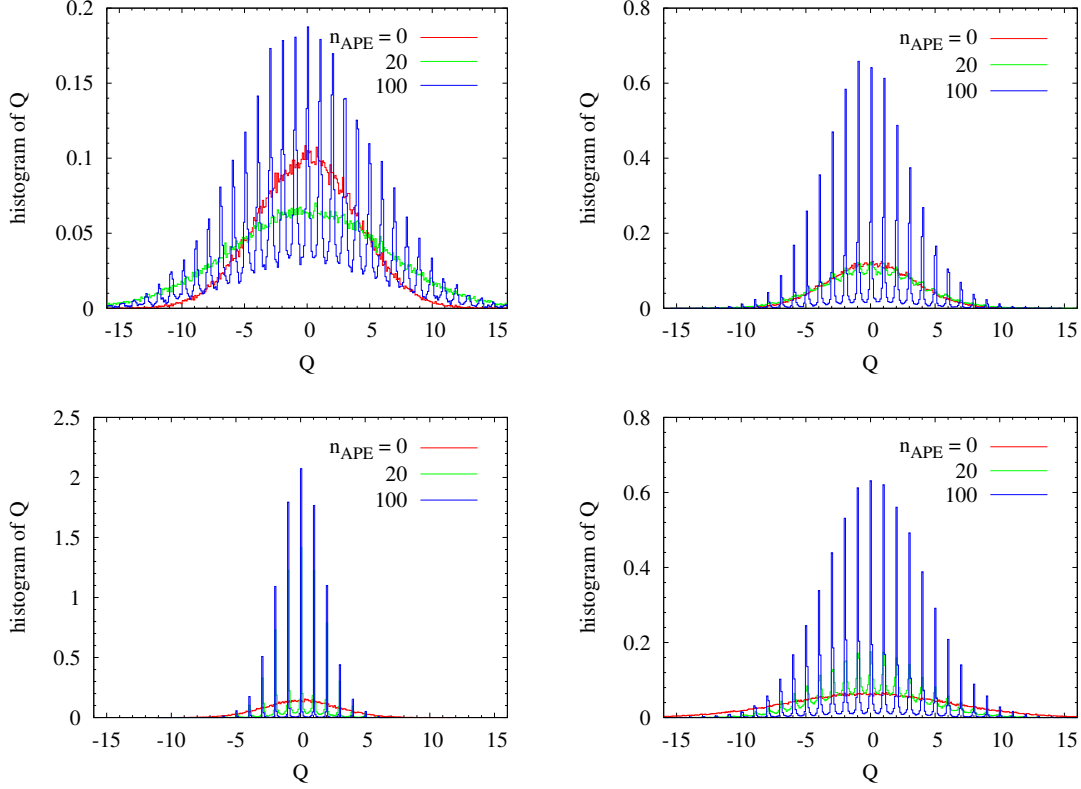


FIG. 7: Histogram of Q for four ensembles at $n_{\text{APE}} = 0, 20, 100$.

possible size of the scaling violation. Indeed, it turns out that these two extrapolations yield smallest and largest values for χ/T_c^4 among other reasonable choices and thus the difference provides with the conservative estimate for the scaling violation.

As the continuum limit of χ/T_c^4 , we obtain 0.200(1) and 0.238(3) for the constant and linear fit, respectively. The difference is due to the large deviation at the coarsest lattice from those at finer lattices, and is interpreted as the potential size of the scaling violation. As for b_2 , the constant and linear fits lead to $-0.049(14)$ and $-0.043(27)$, respectively, and

β	N_S	$a^4\chi(0) \times 10^4$	$c_1 \times 10^7$	$b_2(0) \times 10^2$
1.750	16	3.08(2)	-9.4(3)	-5(5)
1.850	16	1.10(1)	-1.8(1)	-6(3)
1.975	16	0.269(8)	-0.22(2)	-4(2)
1.975	24	0.254(3)	-0.20(1)	-7(4)

TABLE II: Fit results.

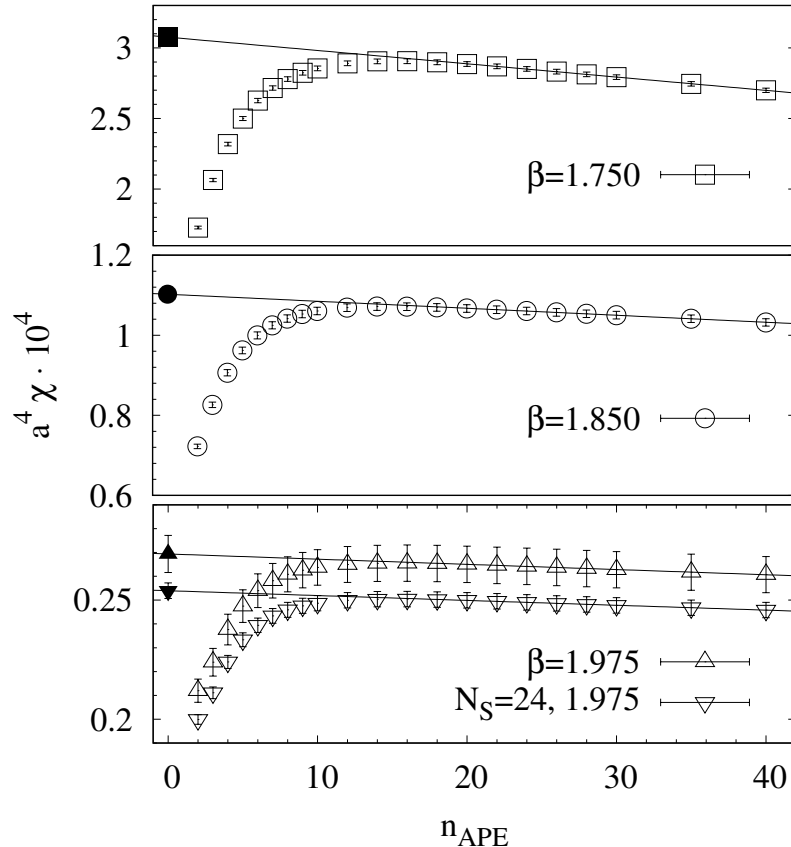


FIG. 8: $a^4\chi$ for the four ensembles as a function of n_{APE} .

the statistical error turns out to dominate the systematic one.

The final results thus obtained are

$$\frac{\chi}{T_c^4} = 0.200(39) , \quad \frac{\chi^{1/4}}{T_c} = 0.674(31) , \quad b_2 = -0.049(20) , \quad (18)$$

where the constant fit is used to estimate the central value and the statistical and the systematic errors are summed in linear.

Further conservative error estimate may be possible by taking the statistical error of the linear fit for b_2 as the final uncertainty. On the other hand, the statistical uncertainty is, in general, expected to increase with complexity of functional form, which could result in overestimate of uncertainty. Since b_2 behaves as a constant, we here adopt the constant fit to provide the representative statistical uncertainty.

In Refs. [14–16], the topological susceptibility χ is calculated in $SU(N)$ gauge theory with several values of N to study the large N behavior. In Refs. [14, 37, 43–45], χ is estimated

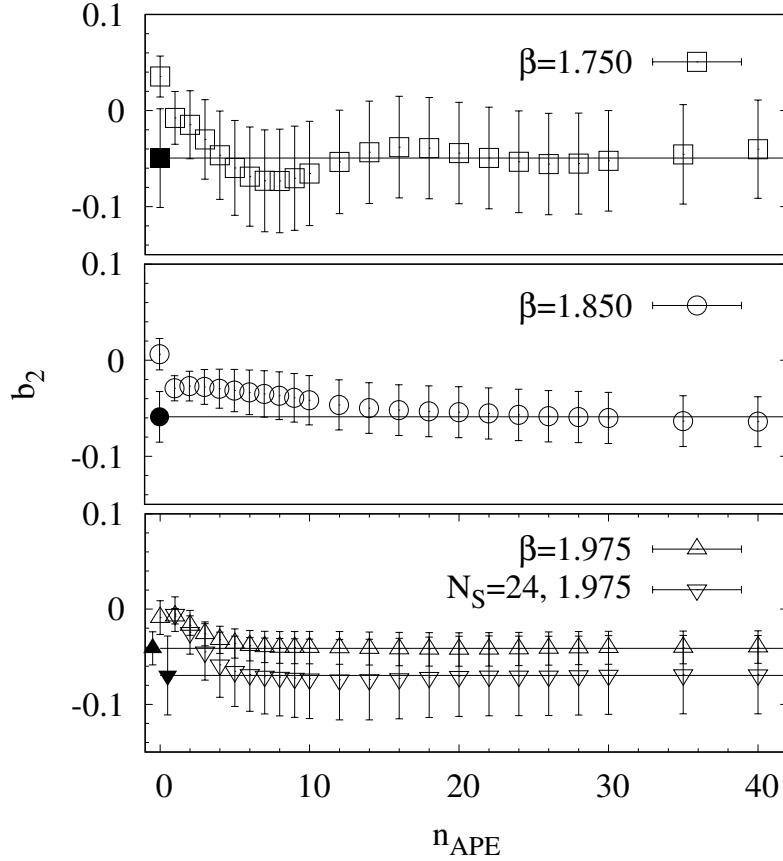


FIG. 9: n_{APE} dependence of b_2 .

for SU(2) gauge theory. As for b_2 , the N dependence is studied for $N \geq 3$ in Refs. [15, 16]. No result is available in the continuum limit for $N = 2$.³ Fig. 11 shows the summary plot for $\chi/\sigma_{\text{str}}^2$ and b_2 , including our results. In this plot, we use $T_c/\sqrt{\sigma_{\text{str}}} = 0.7091(36)$ [32] to change the normalization to $\chi/\sigma_{\text{str}}^2$. The solid lines shown in the plots are the linear fit performed in Ref. [16] using the data at $N = 3, 4, 6$.

The results of χ/σ_{str} for SU(2) theory are slightly above than the solid line, but the deviation is accountable by the next leading order correction, which is of $O(1/N^2)$ relative to the leading one. It is then natural to expect that the dynamics of SU(2) gauge theory is a smooth extrapolation of the large N dynamics to $N = 2$, and that nothing special happens in between.

The value of b_2 at $N = 2$ obtained in this work turns out to be consistent with the

³ See, for an exploratory study, Ref. [46].

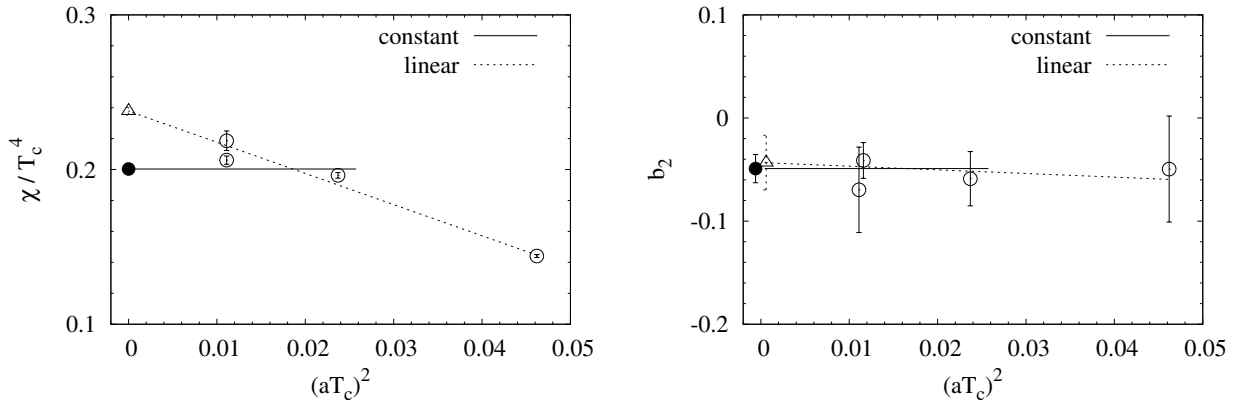


FIG. 10: The continuum limit of χ/T_c^4 and b_2 . The solid lines in both plots are the results from a constant fit using only two finer lattices, and the dashed lines are those from a linear fit using all lattices.

instanton prediction, $b_2^{\text{DIGA}} = -1/12$, within 1.7σ . However, it is more consistent with the naive linear extrapolation from the $N \geq 3$ data to $N = 2$. This observation gives further support to the above expectation, *i.e.* nothing special happens between $N \geq 3$ and $N = 2$. Notice that, in Ref. [47] $b_4 = 6(2) \times 10^{-4}$ is obtained in the continuum limit, which clearly differs from the value predicted from the instanton calculus, $b_4^{\text{DIGA}} = 1/360$.

III. DISCUSSION

A. Large N versus Small N

One of the motivations for present analysis of the 4d $SU(2)$ pure Yang-Mills theory is to study the $SU(N)$ Yang-Mills theories for finite values of N . We expect that $SU(N)$ Yang-Mills theories show qualitatively different behaviors, for large N and for small N .

1. Large N

In the large N limit, the values of the coefficients b_{2i} scales at $O(N^{-2i})$ (6), and hence becomes smaller as N becomes large. This indicates that the vacuum energy, $E(\theta, N)$, will no longer be a 2π -periodic function of θ . While this seems to be in tension with the 2π -periodicity of θ in the Lagrangian, the apparent inconsistency is resolved by the possibility

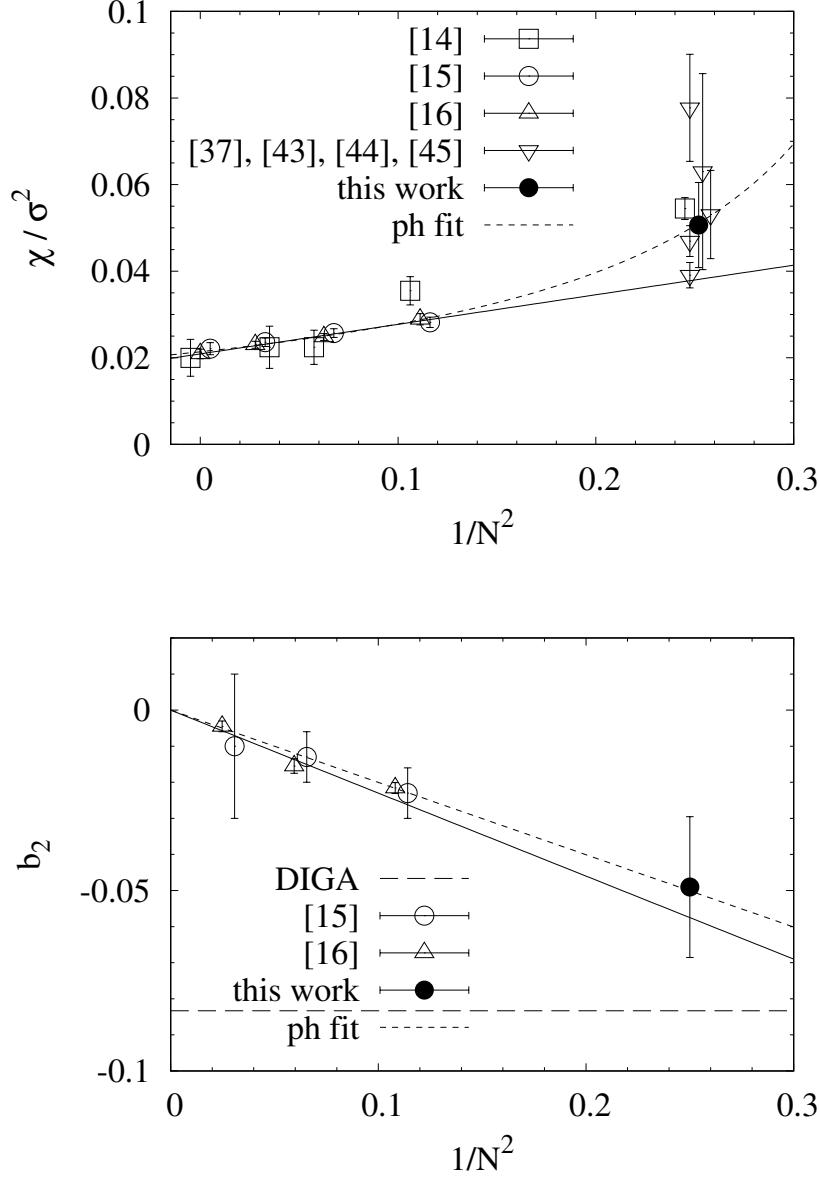


FIG. 11: The N dependence of $\chi/\sigma_{\text{str}}^2$ and b_2 , where the numbers in the legend denote the reference numbers. Each data point is slightly shifted horizontally to make it easier to see. The horizontal dashed line in the b_2 plot represents the dilute instanton gas approximation (DIGA).

that the vacuum energy $E(\theta, N)$ is a multi-valued function of θ [1, 3]. Namely, there are multiple branches $\tilde{E}(\theta + 2\pi n)$ labeled by an integer n , where each $\tilde{E}(\theta)$ has a quadratic potential near $\theta \sim 0$ and has a plateau of height $O(\Lambda^4)$ as $\theta \rightarrow \pm\infty$, with Λ being the

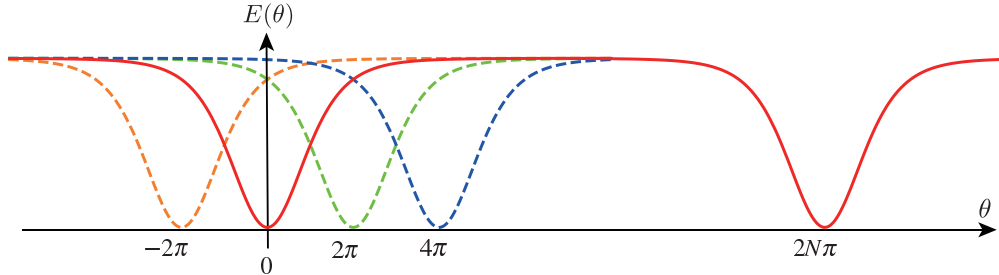


FIG. 12: Schematic picture for the multi-valued vacuum energy for the large N pure Yang-Mills theory, reproduced from Ref. [48].

dynamical scale. The correct minimal energy (over all the branches) is then

$$E(\theta) = \min_{n \in \mathbb{Z}} \tilde{E}(\theta + 2\pi n), \quad (19)$$

see Fig. 12. This in particular means that there are two different lowest-energy states for $\theta = \pi$ mapped each other under the CP symmetry, and hence we expect CP to be spontaneously broken.

One should notice that the vacuum energy takes a different functional form as expected from the semiclassical one-instanton calculation [49], which gives the free energy density as

$$E(\theta) \sim \int_0^\infty \frac{d\rho}{\rho^5} (\mu\rho)^{b_1} \exp\left[-\frac{8\pi^2}{g^2(\mu)}\right] (1 - \cos\theta). \quad (20)$$

Here ρ is the size modulus of the instanton, $g(\mu)$ is the running gauge coupling constant at the energy scale μ , and $b_1 := 11N/3$ is the coefficient of the one-loop beta function.

One of the reasons for the discrepancy between the semi-classical instanton analysis and the large N analysis resides in the famous IR divergence of the instanton analysis: the integral (20) is divergent as ρ becomes large.

2. Small N

The situation can be different when N is small. Let us regard N as a real parameter. Then the integral (20) has a UV divergence at $\rho \rightarrow 0$, if the values of N is smaller than the threshold value $N_{\text{inst}} = 12/11$ [50]. In this case, the integral (20) should be regularized in the UV by the cutoff scale M , so that the lower value of the integral for ρ is given by M^{-1} . Note that the UV regularization is needed even though the pure Yang-Mills theory in itself is asymptotic free.

We thus expect that the one-instanton contribution to have the schematic expression

$$E(\theta, N) \sim M^{4-\frac{11N}{3}} \Lambda^{\frac{11N}{3}} (1 - \cos \theta) , \quad (21)$$

where Λ is the dynamical scale of the theory. This is a different qualitative behavior as suggested by the large N analysis, (19).⁴

There can be several questions to this narrative. First, in the analysis above for small N , we evaluated only the instanton corrections, and one might object that there can be many other contributions to the partition function. While this is certainly true, let us note that these non-instanton contributions give rise to contributions of $O(\Lambda^4)$. Since the cutoff scale M is much larger than the dynamical scale Λ ($M \gg \Lambda$), these non-instanton contributions are much smaller than the instanton contribution of (21). Since we do know that instanton contributes to the path integral, we are certain that there is contribution of the form (21), which we expect will dominate over other contributions.⁵

Note that the UV cutoff M dependence will appear only as an overall divergence. This means that while the topological susceptibility depends on the UV cutoff, the coefficients b_{2i} do not depend on the UV cutoff. This is in fact an advantage of the definition of b_{2i} in (1).

Another possible objection is that it does not make sense to consider non-integer values of N ; $SU(N)$ theory in the conventional thinking is defined only for integers $N \geq 2$. For our purposes, however, it is useful to promote N to be a real parameter and discuss the vacuum energy $E(\theta, N)$ as a function of real values of N as well as θ . Mathematically, one might worry that there are huge ambiguities in extending the functions $E(\theta, N)$ to non-integer values. Indeed, when we multiply the vacuum energy by an expression $F(\sin \pi N)$ for any function $F(x)$ with $F(x = 0) = 1$, the integer values of $E(\theta, N)$ will be preserved. This however changes the asymptotic behavior as $N \rightarrow \infty$. There is a mathematical theorem [54] which guarantees that two real-valued functions, with suitable asymptotic conditions at infinity and with the same values at all integers, coincide. Such considerations are actually

⁴ While we discuss only pure Yang-Mills theory in this paper, similar issue arises for the $SU(2)$ electroweak gauge group for the standard model, and we need to introduce the UV regulator for the small-size instantons. Interestingly, the size of the resulting integral could explain the smallness of the cosmological constant [51–53].

⁵ There can be still multi-instanton corrections. These subleading corrections preserve the 2π -periodicity and hence the CP symmetry, and does not play important roles in what follows.

implicit in the large N analysis, and makes it possible to discuss small non-integer values of N (even to $N < 2$). The threshold value N_{inst} for the instanton calculus makes sense in this context.

3. Intermediate N

We have seen that $\chi \sim O(N^0)$ and $b_{2i} \sim O(N^{-2i})$ for large N while χ depends on UV-cutoff and $b_{2i} \sim b_{2i}^{\text{DIGA}}$ for small N .

What happens at intermediate values of N ? For generic values of θ we do not necessarily expect a sharp transition between “large” and “small” N : there is no good order parameter. The situation is different for the special value of $\theta = \pi$, which has the CP symmetry in the Lagrangian. In this case, we can define two phases by the presence or the absence of the CP symmetry; the CP symmetry is spontaneously broken for large N , while for smaller N the vacuum energy may be given by the cosine form and hence CP is preserved. In that case, there exists a critical value of $N = N_{\text{CP}}$ between the two phases.

We expect that the two phases are different also in that whether the vacuum is gapped or gapless. This is because of the mixed anomaly between the \mathbb{Z}_N center symmetry and the CP symmetry [6], and the presence of the \mathbb{Z}_N symmetry can be regarded as a definition of the confinement. Possible phase diagrams are shown in Fig. 13, where the presence/absence of the CP symmetry is assumed to coincide with the gapped/gapless system. Of course, the presence of the mixed anomaly only shows that at least either the center symmetry or the CP symmetry should be broken, and allows for the possibility that both are broken.

Here, the existence of N_{CP} is our assumption motivated by the phase structure of the CP^{N-1} model we discuss below. Once it is assumed, we need to discuss how the gapless phase extends to the $\theta \neq \pi$ region. In the figure, we show a possibility that the gapless theory is realized even at $\theta = 0$ at some N . There are other possibilities that the line does not reach to $\theta = 0$ axis, as well as the possibility that gapless theories are realized only on the $\theta = \pi$ line. Note that irrespective of the possible phase structures we define the critical value N_{CP} by the presence/absence of the CP symmetry.

Note that the value of N_{inst} is not necessarily the same as the critical value N_{CP} ; the former is defined purely for the semiclassical instanton computation applicable for generic values of θ , while the critical value N_{CP} is the value separating the CP broken/preserved

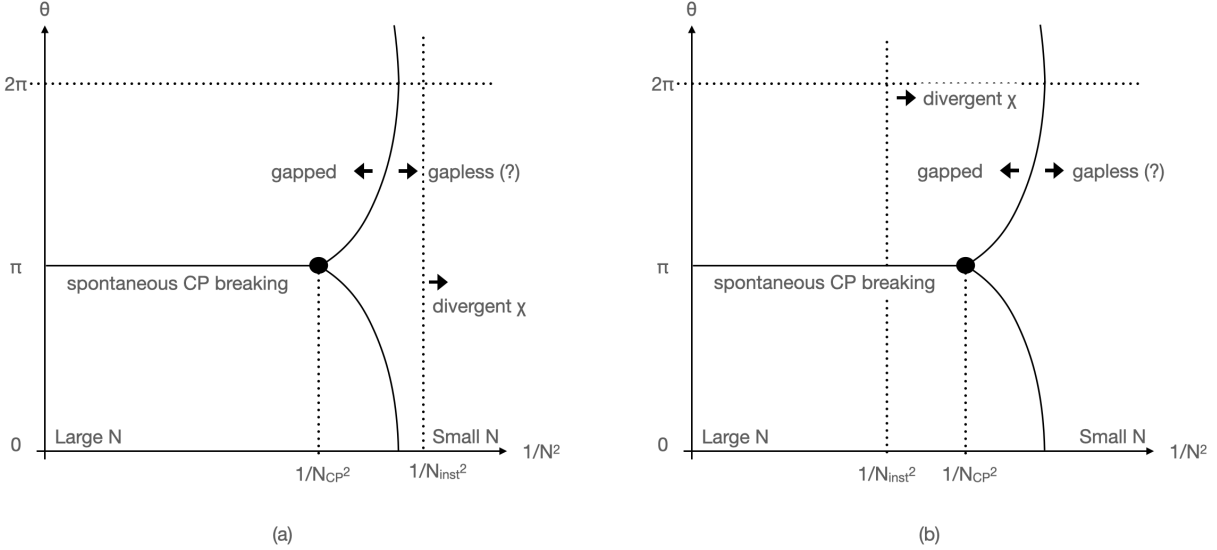


FIG. 13: Possible phase structures of 4d $SU(N)$ pure Yang-Mills theory as a function of $1/N^2$ and θ . At $\theta = \pi$ and $N > N_{CP}$, there is a first-order phase transition. If such N_{CP} exists, a gapless theory should be realized for $N < N_{CP}$ at $\theta = \pi$. Such a region may extend to $\theta \neq \pi$ as in the figures although it is totally unknown. The topological susceptibility, χ , diverges for $N < N_{inst} = 12/11$ by the contributions from small instantons. In (a) and (b) we show possible phase structures where $N_{inst} < N_{CP}$ and $N_{inst} > N_{CP}$, respectively. The mixed anomaly in itself allows for more complicated phase structures, and for example allows regions where both CP and center symmetries are broken.

phases at the special value $\theta = \pi$. It is not a priori clear if we expect general inequalities between the two values N_{inst} and N_{CP} . One may be tempted to imagine that N_{inst} should always be smaller than N_{CP} since the potential generated by the instanton is always smooth so that the spontaneous CP breaking does not happen. However, although it is certain that the contributions from the small instantons dominate the instanton density for $N < N_{inst}$, one cannot exclude the possibility that non-trivial infrared physics still leads the spontaneous CP breaking and/or confinement at $\theta = \pi$.

Let us next come to more quantitative aspects. In the instanton calculus, we obtained the threshold value of $N_{inst} = 12/11$, which is smaller than $N = 2$. The estimation by the one-loop beta function is justified by the asymptotic freedom. Therefore, it is expected that the $SU(2)$ gauge theory has a UV-independent value of the topological susceptibility. As we discussed already, however, one cannot conclude whether $N_{CP} < 2$ holds or not only from

this discussion. Below, we examine the lattice results of the θ -dependence of the theory and discuss whether $N = 2$ is small or large more carefully.

4. Comparison with the CP^{N-1} Model

It is useful to compare the 4d Yang-Mills theory with the celebrated CP^{N-1} model in two dimensions [18, 19]. This theory has many similarities with the 4d $SU(N)$ Yang-Mills theory, and could be of help in understanding the non-perturbative properties of the latter.⁶

In the large N limit of the 2d CP^{N-1} model, there exists gap at any values of θ , and the vacuum energy is discontinuous at $\theta = \pi$, where the CP symmetry is spontaneously broken. There seems to be a consensus that these properties takes over down to $N = 3$. The situation is different from the $N = 2$ case, *i.e.* the CP^1 model, which is nothing but the $O(3)$ spin model. This model is believed to be gapless and have continuous vacuum energy at $\theta = \pi$ [56].

When we consider N as a continuous parameter again, one expects that there will be a critical value of N between the two phases, which we denote by N_{CP} . For $N > N_{CP}$ the theory has spontaneous CP breaking at $\theta = \pi$, and we expect that the dependence on the parameter N is accounted by the large N scaling: we call this the “large N phase.” By contrast for $N < N_{CP}$ we have an unbroken CP symmetry for $\theta = \pi$, and the semiclassical instanton analysis applies: we call this the “small N phase.” The computation similar to (20) gives the threshold value $N_{inst} = 2$ for the CP^{N-1} model, consistent with the divergence of topological susceptibility for the CP^1 -model.

The most remarkable difference of the CP^1 model from other ($N > 2$) CP^{N-1} models is that the semi-classical calculation of the former leads to a UV divergence in the topological susceptibility. This is supported by lattice numerical calculations, unless a suitable counter term is added [50, 57–64]⁷.

⁶ In 2d CP^{N-1} a confining linear potential appears even when instanton dominates the dynamics [55, 56].

⁷ See also Ref. [65], in which the divergence of the topological susceptibility is examined in detail.

B. Quantitative Analysis of Lattice Results

1. $N = 2$

We have already seen that the semi-classical estimate of the topological susceptibility χ in 4d $SU(N)$ gauge theory does not yield UV divergence even for the possible smallest value, $N = 2$. The continuum limit of lattice numerical calculations serves as an independent quantitative test of this expectation.

Although an extrapolation of numerical data is always subtle, and especially the continuum limit of quantities related to topological charge needs special care, our result as well as previous results in the literature demonstrate the finiteness of χ for $SU(N)$ gauge theory, all the way to the value $N = 2$.

As shown in Fig. 11, the magnitude of $|b_2|$ obtained for $N = 2$ is slightly smaller than that of the instanton prediction $b_2^{\text{DIGA}} = -1/12$. The value of $|b_4|$ in Ref. [47] is much smaller than the instanton value. Both are rather consistent with the $1/N^2$ and $1/N^4$ scalings of the $N \geq 3$ data as we discuss further below. This suggests the invalidity of the instanton description. One also expects that the vacuum energy has a cusp at $\theta = \pi$ due to small values of $|b_2|$ and $|b_4|$. All these results suggest that $N = 2$ is “large” for the four-dimensional Yang-Mills theory.

In the literature there have been some attempts to analyze the vacuum of the 4d $SU(2)$ theory at $\theta = \pi$. For example, Ref. [66] analyzes the question for a suitable double-trace deformation of the 4d Yang-Mills theory via the semiclassical analysis and a twisted compactification, and obtained the results consistent with ours. It should be kept in mind, however, that any deformation of the theory, often needed for the semiclassical analysis, could potentially change the vacuum structure of the theory, let alone the precise values of N_{inst} and N_{CP} . It is also the case that for our discussion it is crucial to discuss the transition between small N and large N behaviors, as we will discuss a few paragraphs below.

Our result should be contrasted with the case of the 2d CP^{N-1} model, where $N = 2$ case is gapless and CP preserving at $\theta = \pi$, as already mentioned before. This is an excellent demonstration of the quantitative differences between four-dimensional Yang-Mills theory and the two-dimensional CP^{N-1} model.

Notice that the relation between the 4d $SU(N)$ Yang-Mills theory and the 2d CP^{N-1} model

was further clarified in [67], which showed that the $T^2 \times S^1$ compactification of the former with suitable 't Hooft magnetic flux gives rise to S^1 compactification of the two-dimensional sigma model whose target space has the topology of CP^{N-1} (see Refs. [9, 10] for further checks via anomalies). A caution is needed, however, before any quantitative comparisons between the two. The two-dimensional model obtained from four-dimensional theory has a non-standard metric, and in addition there are special points (fixed points under the Weyl group action) in the CP^{N-1} where we encounter W-bosons of the four-dimensional theory [67]. Moreover for the analysis of [67] it was crucial to have a hierarchy of scales between the sizes of T^2 and S^1 , and any discussion of the standard flat space limit (where there is no such hierarchy) requires careful analytic continuation. These subtleties can easily affect quantitative discussions here.

2. N_{inst}

Once we are settled with the case of $N = 2$, we can discuss even smaller values of N and ask how the theory approaches the $N < N_{\text{inst}}$ region.

We first pretend that N_{inst} is unknown and try to determine its value by the lattice data by two methods. The first method uses topological susceptibility, which we expect to diverge at the value $N = N_{\text{inst}}$. To determine this value we fit our $N = 2$ result together with those for $N = 3, 4, 6$ in Ref. [16] by an Ansatz

$$\frac{\chi}{\sigma_{\text{str}}^2} = \frac{\chi}{\sigma_{\text{str}}^2} \Big|_{N=\infty} \times \frac{N^2}{N^2 - N_{\text{inst}}^2}, \quad (22)$$

where N_{inst} is assumed to be a real number. Here the Ansatz is the simplest function of N^2 which has divergence at $N = N_{\text{inst}}$ and approaches to the large N value as $N \rightarrow \infty$.⁸ We then obtain

$$\frac{\chi}{\sigma_{\text{str}}^2} \Big|_{N=\infty} = 0.0214(2), \quad N_{\text{inst}} = 1.52(10) \quad \text{with } \chi^2/\text{dof} = 0.05 \quad (23)$$

⁸ Our Ansatz is motivated by the analysis performed in Ref. [47], where the topological susceptibilities of 2d CP^{N-1} model are calculated at several values of N and fitted to the function including $1/(N-2)$. Our overall conclusion is qualitatively unchanged if we modify this Ansatz. Note that the possible data points are rather limited, since we have only $N = 2, 3, \dots$, and all the points for $N \geq 3$ are already well-fitted by the large N scaling.

which is shown as the dashed curve in Fig. 11 denoted by “ph fit” meaning phenomenological fit.

The second method uses the values of b_2 . Supposing that the semi-classical calculation becomes valid at $N = N_{\text{inst}}$ for $SU(N)$ gauge theory, b_2 is expected to take $b_2^{\text{DIGA}} = -1/12$ at the same value of N . We again use the results for b_2 for $N = 2, 3, 4, 6$ to test this expectation. This time, by fitting the data to

$$b_2(N) = \frac{b_2^{(1)}}{N^2}, \quad (24)$$

we obtain

$$b_2^{(1)} = -0.200(12) \quad \text{with } \chi^2/\text{dof} = 0.97. \quad (25)$$

Substituting (23) and (25) into (24) yields $b_2(N_{\text{inst}}) = -0.087(5)$, which is consistent with $-1/12$. Furthermore, assuming the functional form of $b_4(N) = b_4^{(1)}/N^4$ and using the result $b_4 = 6(2) \times 10^{-4}$ at $N = 2$ [47], $b_4(N_{\text{inst}}) = 0.0018(6)$ is obtained, which is not that far from $b_4^{\text{DIGA}} = 1/360$.

The two methods produce consistent estimates $N_{\text{inst}} \sim 1.5$, slightly larger than the semi-classical value $12/11$. This numerology serves as a check of the overall picture, and moreover indicates that the large N scaling of b_2 holds well all the way until the value $N \sim N_{\text{inst}}$, where χ diverges. If we assume large N scaling for all the b_{2n} 's until $N \sim N_{\text{inst}}$, then certain derivatives of the free energy are necessarily discontinuous at $\theta = \pi$, thus implying the breaking of the CP symmetry. This suggests the inequality $N_{\text{CP}} \lesssim N_{\text{inst}}$. Further numerical studies are needed to make this inequality more precise.

Summarizing our discussion, the numerical data suggests the following shape of the vacuum energy density, as we change the value of N . At large N we have the quadratic form of the vacuum energy around $\theta = 0$, while there is a cusp at $\theta = \pi$. As we change N to smaller values, b_2 and b_4 grow while continue to obey the large N scaling to a good approximation. The cusp of the vacuum energy at $\theta = \pi$ is gradually smoothed, however not completely; CP is still spontaneously broken. The transition of the large N picture to the instanton picture seems to be smooth as far as b_{2n} are concerned, and $N = 2$ is on the “large N ” side. At $N_{\text{inst}} \sim 1.5$ the free energy approaches the cosine function with a diverging overall factor, χ . Once χ is diverging, it becomes difficult to infer the vacuum structure from the vacuum energy only, since the vacuum energy is masked by the large contributions of small

instantons. In particular, it becomes invisible in practice whether or not there is a phase transition at $\theta = \pi$.

IV. SUMMARY AND DISCUSSION

We performed lattice numerical simulations to explore the θ dependence of the vacuum energy in 4d SU(2) pure Yang-Mills theory, with special attention to the response of topological excitation to the smearing procedure. We discussed the method to extract the topological information from smeared configurations properly and estimated the first two coefficients in the θ expansion of the vacuum energy in the continuum limit, namely χ and b_2 . The value of χ turns out to be consistent with the previous results in the literature, while b_2 is determined for the first time.

We use these results to infer the phase structure of the 4d SU(N) theory as we change the values of N and θ . We highlighted the differences for “large N ” and for “small N ”: we have the large N scaling for the former, while the vacuum energy is dominated by instantons in the latter. The differences between the two is most clear-cut for $\theta = \pi$, where the CP symmetry is spontaneously broken for large N , while unbroken for small N .

We found that for $N = 2$ the topological susceptibility χ remains finite, and b_2 slightly deviates from the instanton predictions, while it is well fitted by the $1/N^2$ extrapolation from the $N \geq 3$ values. By further extrapolating N to small values by analytic continuation, we find that χ and b_2 reach the instanton predictions at $N_{\text{inst}} = 1.52(2)$, and that the free energy will be dominated by instantons.

Our analysis gives strong quantitative evidence that the SU(2) theory, and hence all SU(N) theories for integer N , are in the large N category. While large N analysis is often regarded as an approximation applicable only to the large values of N , our results suggest that the large N analysis is more powerful, and can be useful for studying all possible values of N , even as small as $N = 2$. This is in contrast with the case of the 2d CP $^{N-1}$ model, which is believed to be gapless for $N = 2$, while are gapped for $N \geq 3$. It would be interesting to study for more general theories the applicability of large N analysis to smaller values of N .

In this work, we could not explore the question of precisely what topological object carries non-zero topological charges. In Ref. [40], it was pointed out that in SU(3) Yang-Mills theory the codimension-one objects (“sheets”) are responsible for the non-zero topological charges,

and from the similar study of CP^{N-1} model it was pointed out that the object becomes localized and becomes instantons as $N \rightarrow N_{CP}$. Thus, it is interesting to see what objects are responsible for the topological charges in the 4d $SU(2)$ theory.

It is also interesting to see the θ dependence of the vacuum energy directly on the lattice, for finite real values of θ , especially near $\theta = \pi$. This program has to overcome notoriously difficult problem, the sign problem. Since recent development in methodology is remarkable [11–13], such direct studies appear to be within reach in the near future.

Finally, it is interesting to ask if the analysis of this paper has any phenomenological considerations of the dynamical θ -angle, the axion [68–71]. For example, in the axionic inflationary models of Ref. [72] (see also Ref. [73]), the values of b_{2n} affect future observations of primordial gravitational waves from inflation [48].

Acknowledgments

We would like to thank Hideo Matsufuru and Julien Frison for the support on developing the codes used in this work, and Aleksey Cherman for discussion. This work is in part based on Bridge++ code (see, for details, <http://bridge.kek.jp/Lattice-code/> and Ref. [74]), and supported by JSPS KAKENHI Grant-in-Aid for Scientific Research (Nos. 19H00689 [RK, NY, MY], 18K03662 [NY], 19K03820 [MY]) and MEXT KAKENHI Grant-in-Aid for Scientific Research on Innovative Areas (No. 18H05542 [RK]). Numerical computation in this work was carried out in part on the Oakforest-PACS and Cygnus under Multidisciplinary Cooperative Research Program (No. 17a15) in Center for Computational Sciences, University of Tsukuba; the Yukawa Institute Computer Facility, Yukawa Institute, Kyoto University; a supercomputer (NEC SX-5) at Research Center for Nuclear Physics, Osaka University; Fujitsu PRIMERGY CX600M1/CX1640M1 (Oakforest-PACS) in the Information Technology Center, The University of Tokyo.

-
- [1] E. Witten, “Large N Chiral Dynamics,” *Annals Phys.* **128**, 363 (1980)
doi: 10.1016/0003-4916(80)90325-5
 - [2] G. ’t Hooft, “Topology of the Gauge Condition and New Confinement Phases in Nonabelian Gauge Theories,” *Nucl. Phys. B* **190**, 455-478 (1981) doi: 10.1016/0550-3213(81)90442-9

- [3] E. Witten, “Theta dependence in the large N limit of four-dimensional gauge theories,” Phys. Rev. Lett. **81**, 2862-2865 (1998) doi: 10.1103/PhysRevLett.81.2862 [arXiv:hep-th/9807109 [hep-th]].
- [4] G. 't Hooft, “A Planar Diagram Theory for Strong Interactions,” Nucl. Phys. B **72**, 461 (1974) doi: 10.1016/0550-3213(74)90154-0
- [5] D. Gaiotto, A. Kapustin, N. Seiberg and B. Willett, “Generalized Global Symmetries,” JHEP **02**, 172 (2015) doi: 10.1007/JHEP02(2015)172 [arXiv:1412.5148 [hep-th]].
- [6] D. Gaiotto, A. Kapustin, Z. Komargodski and N. Seiberg, “Theta, Time Reversal, and Temperature,” JHEP **05**, 091 (2017) doi: 10.1007/JHEP05(2017)091 [arXiv:1703.00501 [hep-th]].
- [7] R. Kitano, T. Suyama and N. Yamada, “ $\theta = \pi$ in $SU(N)/\mathbb{Z}_N$ gauge theories,” JHEP **09**, 137 (2017) doi: 10.1007/JHEP09(2017)137 [arXiv:1709.04225 [hep-th]].
- [8] V. Azcoiti, A. Galante and V. Laliena, “Theta vacuum: Phase transitions and / or symmetry breaking at theta = pi,” Prog. Theor. Phys. **109**, 843-851 (2003) doi: 10.1143/PTP.109.843 [arXiv:hep-th/0305065 [hep-th]].
- [9] M. Yamazaki, “Relating 't Hooft Anomalies of 4d Pure Yang-Mills and 2d $\mathbb{C}\mathbb{P}^{N-1}$ Model,” JHEP **10**, 172 (2018) doi: 10.1007/JHEP10(2018)172 [arXiv:1711.04360 [hep-th]].
- [10] Z. Wan, J. Wang and Y. Zheng, “New higher anomalies, SU(N) Yang-Mills gauge theory and $\mathbb{C}\mathbb{P}^{N-1}$ sigma model,” Annals Phys. **414**, 168074 (2020) doi: 10.1016/j.aop.2020.168074 [arXiv:1812.11968 [hep-th]].
- [11] M. Hirasawa, A. Matsumoto, J. Nishimura and A. Yosprakob, “Complex Langevin analysis of 2D U(1) gauge theory on a torus with a θ term,” [arXiv:2004.13982 [hep-lat]].
- [12] C. Gattringer and O. Orasch, “Density of states approach for lattice gauge theory with a θ -term,” Nucl. Phys. B **957**, 115097 (2020) doi: 10.1016/j.nuclphysb.2020.115097 [arXiv:2004.03837 [hep-lat]].
- [13] T. Sulejmanpasic, D. D. Goschl and C. Gattringer, “First-principle simulations of 1+1d quantum field theories at $\theta = \pi$ and spin-chains,” [arXiv:2007.06323 [cond-mat.str-el]].
- [14] B. Lucini and M. Teper, “SU(N) gauge theories in four-dimensions: Exploring the approach to $N = \infty$,” JHEP **06**, 050 (2001) doi: 10.1088/1126-6708/2001/06/050 [arXiv:hep-lat/0103027 [hep-lat]].
- [15] L. Del Debbio, H. Panagopoulos and E. Vicari, “theta dependence of SU(N) gauge theories,” JHEP **08**, 044 (2002) doi: 10.1088/1126-6708/2002/08/044 [arXiv:hep-th/0204125 [hep-th]].

- [16] C. Bonati, M. D’Elia, P. Rossi and E. Vicari, “ θ dependence of 4D $SU(N)$ gauge theories in the large- N limit,” *Phys. Rev. D* **94**, no. 8, 085017 (2016) doi: 10.1103/PhysRevD.94.085017 [arXiv:1607.06360 [hep-lat]].
- [17] C. Bonati, M. D’Elia, H. Panagopoulos and E. Vicari, “Change of θ Dependence in 4D $SU(N)$ Gauge Theories Across the Deconfinement Transition,” *Phys. Rev. Lett.* **110**, no.25, 252003 (2013) doi: 10.1103/PhysRevLett.110.252003 [arXiv:1301.7640 [hep-lat]].
- [18] H. Eichenherr, “ $SU(N)$ Invariant Nonlinear Sigma Models,” *Nucl. Phys. B* **146**, 215-223 (1978) doi: 10.1016/0550-3213(79)90287-6
- [19] A. D’Adda, M. Luscher and P. Di Vecchia, “A $1/n$ Expandable Series of Nonlinear Sigma Models with Instantons,” *Nucl. Phys. B* **146**, 63-76 (1978) doi: 10.1016/0550-3213(78)90432-7
- [20] See, for example, B. B. Beard, M. Pepe, S. Riederer and U. J. Wiese, “Study of $CP(N-1)$ theta-vacua by cluster-simulation of $SU(N)$ quantum spin ladders,” *Phys. Rev. Lett.* **94**, 010603 (2005) doi: 10.1103/PhysRevLett.94.010603 [arXiv:hep-lat/0406040 [hep-lat]].
- [21] F. D. M. Haldane, “Nonlinear field theory of large spin Heisenberg antiferromagnets. Semi-classically quantized solitons of the one-dimensional easy Axis Neel state,” *Phys. Rev. Lett.* **50**, 1153-1156 (1983) doi: 10.1103/PhysRevLett.50.1153
- [22] F. D. M. Haldane, “Continuum dynamics of the 1-D Heisenberg antiferromagnetic identification with the $O(3)$ nonlinear sigma model,” *Phys. Lett. A* **93**, 464-468 (1983) doi: 10.1016/0375-9601(83)90631-X
- [23] I. Affleck and F. D. M. Haldane, “Critical Theory of Quantum Spin Chains,” *Phys. Rev. B* **36**, 5291-5300 (1987) doi: 10.1103/PhysRevB.36.5291
- [24] R. Shankar and N. Read, “The $\theta = \pi$ Nonlinear σ Model Is Massless,” *Nucl. Phys. B* **336**, 457-474 (1990) doi: 10.1016/0550-3213(90)90437-I
- [25] I. Affleck, “Nonlinear sigma model at $\Theta = \pi$: Euclidean lattice formulation and solid-on-solid models,” *Phys. Rev. Lett.* **66**, 2429-2432 (1991) doi: 10.1103/PhysRevLett.66.2429
- [26] A. B. Zamolodchikov and A. B. Zamolodchikov, “Massless factorized scattering and sigma models with topological terms,” *Nucl. Phys. B* **379**, 602-623 (1992) doi: 10.1016/0550-3213(92)90136-Y
- [27] W. Bietenholz, A. Pochinsky and U. J. Wiese, “Meron cluster simulation of the theta vacuum in the 2-d $O(3)$ model,” *Phys. Rev. Lett.* **75**, 4524-4527 (1995) doi: 10.1103/PhysRevLett.75.4524 [arXiv:hep-lat/9505019 [hep-lat]].

- [28] B. Alles and A. Papa, “Mass gap in the 2D O(3) non-linear sigma model with a $\theta=\pi$ term,” Phys. Rev. D **77**, 056008 (2008) doi: 10.1103/PhysRevD.77.056008 [arXiv:0711.1496 [cond-mat.stat-mech]].
- [29] B. Alles, M. Giordano and A. Papa, “Behavior near $\theta = \pi$ of the mass gap in the two-dimensional O(3) non-linear sigma model,” Phys. Rev. B **90**, no.18, 184421 (2014) doi: 10.1103/PhysRevB.90.184421 [arXiv:1409.1704 [hep-lat]].
- [30] P. Weisz, “Continuum Limit Improved Lattice Action for Pure Yang-Mills Theory. 1.,” Nucl. Phys. B **212**, 1-17 (1983) doi: 10.1016/0550-3213(83)90595-3
- [31] P. Giudice and S. Piemonte, “Improved thermodynamics of SU(2) gauge theory,” Eur. Phys. J. C **77**, no.12, 821 (2017) doi: 10.1140/epjc/s10052-017-5392-6 [arXiv:1708.01216 [hep-lat]].
- [32] B. Lucini, M. Teper and U. Wenger, “The High temperature phase transition in SU(N) gauge theories,” JHEP **01**, 061 (2004) doi: 10.1088/1126-6708/2004/01/061 [arXiv:hep-lat/0307017 [hep-lat]].
- [33] C. Bonati and M. D’Elia, “Comparison of the gradient flow with cooling in SU(3) pure gauge theory,” Phys. Rev. D **89**, no.10, 105005 (2014) doi: 10.1103/PhysRevD.89.105005 [arXiv:1401.2441 [hep-lat]].
- [34] C. Alexandrou, A. Athenodorou and K. Jansen, “Topological charge using cooling and the gradient flow,” Phys. Rev. D **92**, no.12, 125014 (2015) doi: 10.1103/PhysRevD.92.125014 [arXiv:1509.04259 [hep-lat]].
- [35] C. Alexandrou, A. Athenodorou, K. Cichy, A. Dromard, E. Garcia-Ramos, K. Jansen, U. Wenger and F. Zimmermann, “Comparison of topological charge definitions in Lattice QCD,” Eur. Phys. J. C **80**, no.5, 424 (2020) doi: 10.1140/epjc/s10052-020-7984-9 [arXiv:1708.00696 [hep-lat]].
- [36] M. Albanese *et al.* [APE], “Glueball Masses and String Tension in Lattice QCD,” Phys. Lett. B **192**, 163-169 (1987) doi: 10.1016/0370-2693(87)91160-9
- [37] P. de Forcrand, M. Garcia Perez and I. O. Stamatescu, “Topology of the SU(2) vacuum: A Lattice study using improved cooling,” Nucl. Phys. B **499**, 409 (1997) doi: 10.1016/S0550-3213(97)00275-7 [hep-lat/9701012].
- [38] M. L. Laursen, J. Smit and J. C. Vink, “Small scale instantons, staggered fermions and the topological susceptibility,” Nucl. Phys. B **343**, 522-540 (1990) doi: 10.1016/0550-3213(90)90481-R

- [39] S. O. Bilson-Thompson, D. B. Leinweber, A. G. Williams and G. V. Dunne, “Comparison of $—Q— = 1$ and $—Q— = 2$ gauge-field configurations on the lattice four-torus,” *Annals Phys.* **311**, 267-287 (2004) doi: 10.1016/j.aop.2003.12.011 [arXiv:hep-lat/0306010 [hep-lat]].
- [40] I. Horvath, S. Dong, T. Draper, F. Lee, K. Liu, N. Mathur, H. Thacker and J. Zhang, “Low dimensional long range topological charge structure in the QCD vacuum,” *Phys. Rev. D* **68**, 114505 (2003) doi: 10.1103/PhysRevD.68.114505 [arXiv:hep-lat/0302009 [hep-lat]].
- [41] S. Ahmad, J. T. Lenaghan and H. B. Thacker, “Coherent topological charge structure in $CP(N-1)$ models and QCD,” *Phys. Rev. D* **72**, 114511 (2005) doi: 10.1103/PhysRevD.72.114511 [arXiv:hep-lat/0509066 [hep-lat]].
- [42] Y. Lian and H. B. Thacker, “Small Instantons in CP^{**1} and CP^{**2} Sigma Models,” *Phys. Rev. D* **75**, 065031 (2007) doi: 10.1103/PhysRevD.75.065031 [arXiv:hep-lat/0607026 [hep-lat]].
- [43] B. Alles, M. D’Elia and A. Di Giacomo, “Topology at zero and finite T in $SU(2)$ Yang-Mills theory,” *Phys. Lett. B* **412**, 119-124 (1997) doi: 10.1016/S0370-2693(97)01059-9 [arXiv:hep-lat/9706016 [hep-lat]].
- [44] T. A. DeGrand, A. Hasenfratz and T. G. Kovacs, “Topological structure in the $SU(2)$ vacuum,” *Nucl. Phys. B* **505**, 417-441 (1997) doi: 10.1016/S0550-3213(97)00480-X [arXiv:hep-lat/9705009 [hep-lat]].
- [45] B. A. Berg and D. A. Clarke, “Topological charge and cooling scales in pure $SU(2)$ lattice gauge theory,” *Phys. Rev. D* **97**, no.5, 054506 (2018) doi: 10.1103/PhysRevD.97.054506 [arXiv:1710.09474 [hep-lat]].
- [46] G. Bhanot, E. Rabinovici, N. Seiberg and P. Woit, “LATTICE THETA VACUA,” *Nucl. Phys. B* **230**, 291-298 (1984) doi: 10.1016/0550-3213(84)90214-1
- [47] C. Bonanno, C. Bonati and M. D’Elia, “Topological properties of CP^{N-1} models in the large- N limit,” *JHEP* **01**, 003 (2019) doi: 10.1007/JHEP01(2019)003 [arXiv:1807.11357 [hep-lat]].
- [48] Y. Nomura and M. Yamazaki, “Tensor Modes in Pure Natural Inflation,” *Phys. Lett. B* **780**, 106-110 (2018) doi: 10.1016/j.physletb.2018.02.071 [arXiv:1711.10490 [hep-ph]].
- [49] G. ’t Hooft, “Computation of the Quantum Effects Due to a Four-Dimensional Pseudoparticle,” *Phys. Rev. D* **14**, 3432-3450 (1976) [erratum: *Phys. Rev. D* **18**, 2199 (1978)] doi: 10.1103/PhysRevD.14.3432
- [50] M. Luscher, “Does the Topological Susceptibility in Lattice Sigma Models Scale According to the Perturbative Renormalization Group?,” *Nucl. Phys. B* **200**, 61-70 (1982)

doi: 10.1016/0550-3213(82)90058-X

- [51] Y. Nomura, T. Watari and T. Yanagida, “Quintessence axion potential induced by electroweak instanton effects,” *Phys. Lett. B* **484**, 103-111 (2000) doi: 10.1016/S0370-2693(00)00605-5 [arXiv:hep-ph/0004182 [hep-ph]].
- [52] L. McLerran, R. Pisarski and V. Skokov, “Electroweak Instantons, Axions, and the Cosmological Constant,” *Phys. Lett. B* **713**, 301-303 (2012) doi: 10.1016/j.physletb.2012.05.057 [arXiv:1204.2533 [hep-ph]].
- [53] M. Ibe, M. Yamazaki and T. T. Yanagida, “Quintessence Axion Revisited in Light of Swampland Conjectures,” *Class. Quant. Grav.* **36**, no.23, 235020 (2019) doi: 10.1088/1361-6382/ab5197 [arXiv:1811.04664 [hep-th]].
- [54] F. Carlson, “Sur une classe de séries de Taylor,” Dissertation, Uppsala, Sweden, 1914.
- [55] M. Luscher, “The Secret Long Range Force in Quantum Field Theories With Instantons,” *Phys. Lett. B* **78**, 465-467 (1978) doi: 10.1016/0370-2693(78)90487-2
- [56] P. Keith-Hynes and H. Thacker, “Fractionally charged Wilson loops as a probe of theta-dependence in $CP(N-1)$ sigma models: Instantons vs. large N ,” *Phys. Rev. D* **78**, 025009 (2008) doi: 10.1103/PhysRevD.78.025009 [arXiv:0804.1534 [hep-lat]].
- [57] B. Berg and M. Luscher, “Definition and Statistical Distributions of a Topological Number in the Lattice $O(3)$ Sigma Model,” *Nucl. Phys. B* **190**, 412-424 (1981) doi: 10.1016/0550-3213(81)90568-X
- [58] B. Berg, “Dislocations and Topological Background in the Lattice $O(3)$ σ Model,” *Phys. Lett. B* **104**, 475-480 (1981) doi: 10.1016/0370-2693(81)90518-9
- [59] F. Farchioni and A. Papa, “Heating and small size instantons in the $O(3)$ sigma model on the lattice,” *Nucl. Phys. B* **431**, 686-708 (1994) doi: 10.1016/0550-3213(94)90219-4 [arXiv:hep-lat/9407026 [hep-lat]].
- [60] M. Blatter, R. Burkhalter, P. Hasenfratz and F. Niedermayer, “Instantons and the fixed point topological charge in the two-dimensional $O(3)$ sigma model,” *Phys. Rev. D* **53**, 923-932 (1996) doi: 10.1103/PhysRevD.53.923 [arXiv:hep-lat/9508028 [hep-lat]].
- [61] M. D’Elia, F. Farchioni and A. Papa, “Renormalization group flow and fixed point of the lattice topological charge in the two-dimensional $O(3)$ sigma model,” *Phys. Rev. D* **55**, 2274-2282 (1997) doi: 10.1103/PhysRevD.55.2274 [arXiv:hep-lat/9511021 [hep-lat]].
- [62] R. Burkhalter, M. Imachi, Y. Shinno and H. Yoneyama, “ CP^{N-1} models with theta term

- and fixed point action,” *Prog. Theor. Phys.* **106**, 613-640 (2001) doi: 10.1143/PTP.106.613 [arXiv:hep-lat/0103016 [hep-lat]].
- [63] W. Bietenholz, U. Gerber, M. Pepe and U. J. Wiese, “Topological Lattice Actions,” *JHEP* **12**, 020 (2010) doi: 10.1007/JHEP12(2010)020 [arXiv:1009.2146 [hep-lat]].
- [64] W. Bietenholz, P. de Forcrand, U. Gerber, H. Mejia-Diaz and I. O. Sandoval, “Topological Susceptibility of the 2d O(3) Model under Gradient Flow,” *Phys. Rev. D* **98**, no.11, 114501 (2018) doi: 10.1103/PhysRevD.98.114501 [arXiv:1808.08129 [hep-lat]].
- [65] M. Berni, C. Bonanno and M. D’Elia, “ θ -dependence in the small- N limit of 2d CP^{N-1} models,” [arXiv:2009.14056 [hep-lat]].
- [66] M. Unsal, “Theta dependence, sign problems and topological interference,” *Phys. Rev. D* **86**, 105012 (2012) doi: 10.1103/PhysRevD.86.105012 [arXiv:1201.6426 [hep-th]].
- [67] M. Yamazaki and K. Yonekura, “From 4d Yang-Mills to 2d $\mathbb{C}P^{N-1}$ model: IR problem and confinement at weak coupling,” *JHEP* **07**, 088 (2017) doi: 10.1007/JHEP07(2017)088 [arXiv:1704.05852 [hep-th]].
- [68] R. D. Peccei and H. R. Quinn, “CP Conservation in the Presence of Instantons,” *Phys. Rev. Lett.* **38**, 1440-1443 (1977) doi: 10.1103/PhysRevLett.38.1440
- [69] R. D. Peccei and H. R. Quinn, “Constraints Imposed by CP Conservation in the Presence of Instantons,” *Phys. Rev. D* **16**, 1791-1797 (1977) doi: 10.1103/PhysRevD.16.1791
- [70] S. Weinberg, “A New Light Boson?,” *Phys. Rev. Lett.* **40**, 223-226 (1978) doi: 10.1103/PhysRevLett.40.223
- [71] F. Wilczek, “Problem of Strong P and T Invariance in the Presence of Instantons,” *Phys. Rev. Lett.* **40**, 279-282 (1978) doi: 10.1103/PhysRevLett.40.279
- [72] Y. Nomura, T. Watari and M. Yamazaki, “Pure Natural Inflation,” *Phys. Lett. B* **776**, 227-230 (2018) doi: 10.1016/j.physletb.2017.11.052 [arXiv:1706.08522 [hep-ph]].
- [73] S. Dubovsky, A. Lawrence and M. M. Roberts, “Axion monodromy in a model of holographic gluodynamics,” *JHEP* **02**, 053 (2012) doi: 10.1007/JHEP02(2012)053 [arXiv:1105.3740 [hep-th]].
- [74] S. Ueda, S. Aoki, T. Aoyama, K. Kanaya, H. Matsufuru, S. Motoki, Y. Namekawa, H. Nemura, Y. Taniguchi and N. Ukita, “Development of an object oriented lattice QCD code ‘Bridge++’,” *J. Phys. Conf. Ser.* **523**, 012046 (2014) doi: 10.1088/1742-6596/523/1/012046